(This is a sample cover image for this issue. The actual cover is not yet available at this time.)

Earth and Planetary Science Letters 319-320 (2012) 197–206

Contents lists available at SciVerse ScienceDirect

Earth and Planetary Science Letters

journal homepage: www.elsevier.com/locate/epsl

U–Th–Pb isotope data indicate phanerozoic age for oxidation of the 3.4 Ga Apex Basalt

Weiqiang Li *, Clark M. Johnson, Brian L. Beard

University of Wisconsin-Madison, Department of Geoscience, 1215 West Dayton Street, Madison WI 53706, United States
NASA Astrobiology Institute, United States

ARTICLE INFO

Article history:
Received 7 July 2011
Received in revised form 21 December 2011
Accepted 22 December 2011
Available online 28 December 2011

Editor: R.W. Carlson

Keywords:
U–Th–Pb geochronology
Marble Bar Chert
Apex Basalt, Pilbara Craton
Tertiary deep weathering
U addition
hematite

ABSTRACT

The occurrence of ferric oxides in Archean rocks has played an important role in discussions on the amount of free oxygen in the atmosphere of the ancient Earth. Recognizing that post-Archean weathering may also produce oxide minerals, drill cores have been used to obtain samples beneath the depth of Phanerozoic weathering. The first core of the Archean Biosphere Drilling Project (ABDP-1) documented hematite as alteration products in 3.4 Ga basalts from the Marble Bar area of the Pilbara Craton, NW Australia, and this has been used to infer the presence of an O_2-bearing atmosphere in the Archean. It is possible, however, that despite recovery of samples from >100 m depth, oxidation of the basalts occurred much younger than the depositional age. In this study, the age of oxidation of the Apex Basalt from the ABDP-1 drill core at Marble Bar is constrained by U–Th–Pb geochronology. Lead and U concentrations of the basalts from the ABDP-1 drill core vary greatly, between <1–58 ppm and 0.08–1.04 ppm, respectively, whereas Th contents are more restricted (0.24–0.71 ppm). $^{206}Pb/^{204}Pb$ ratios are non-radiogenic and vary from 12.44 to 14.69. The linear array in terms of $^{206}Pb/^{204}Pb$–$^{207}Pb/^{204}Pb$ variations does not reflect an age but reflects two-component mixing between a non-radiogenic "ore lead" end member and a radiogenic "basalt lead" end member. The samples do not form isochrons on $^{238}U/^{204}Pb$–$^{206}Pb/^{204}Pb$, $^{235}U/^{204}Pb$–$^{207}Pb/^{204}Pb$, or $^{232}Th/^{204}Pb$–$^{208}Pb/^{204}Pb$ diagrams, indicating post-formation U and Pb addition. Comparison of measured U/Th ratios with "model" U/Th ratios calculated based on $^{208}Pb/^{204}Pb$–$^{206}Pb/^{204}Pb$ variations indicates that U enrichment most likely occurred in the last 200 Ma. The degree of U enrichment in the samples is correlated with $Fe^{(III)}/Fe_{Total}$ ratios, indicating that U addition and oxidation were related, most likely reflecting penetration of oxygenated surface waters in the Phanerozoic along bedding planes and shear zones. These results, therefore, indicate that oxidation of the Apex Basalt did not occur in the Archean, and therefore cannot be used to infer an oxygenated atmosphere at that time.

1. Introduction

Evolution of Earth's early atmosphere is critical to understanding the geologic history of the Earth, as well as the origin and evolution of life (e.g., Canfield, 2005). There is extensive literature on the evolution of Earth's atmosphere (e.g., Berkner and Marshall, 1965; Cloud, 1972; Dimroth and Kimberley, 1976; Garrels et al., 1973; Holland, 1984; Kasting, 1993; Walker and Brimblecombe, 1985), yet the levels of oxygen in Earth's atmosphere in the Archean continue to be debated (Holland, 1999; Ohmoto, 1997). A common model proposes that oxygen in the atmosphere was absent or very low until the Great Oxidation Event between 2.45 Ga and 2.22 Ga (e.g., Holland, 2006). Evidence supporting this model includes large mass-independent fractionation of sulfur isotopes (MIF-S) in geological samples older than 2.45 Ga (Farquhar et al., 2000, 2007), although the interpretation of MIF-S as an indicator of atmospheric O_2 level has been questioned (Ohmoto et al., 2006; Watanabe et al., 2009). The mineralogical record has also been used to constrain early Earth's atmospheric O_2 levels, where, for example, preservation of detrital uraninite and siderite in Archean samples has been used to infer low oxygen contents prior to the Great Oxidation Event (e.g., Rasmussen and Buick, 1999). Contrasting arguments have been put forth for hematite that occurs in chert (jasper) from the 3.4 Ga old Marble Bar Chert Member (MBC) in the Pilbara Craton, Western Australia, which has been used to argue that Earth's early atmosphere contained significant amounts of oxygen (Hoashi et al., 2009).

A key issue in using iron oxide minerals in Archean rocks to infer high O_2 levels in Earth's early atmosphere is whether the oxides were produced by recent oxidation. Hoashi et al. (2009) interpreted hematite from the MBC to have formed 3.4 Ga ago, in part because the samples were recovered from depths greater than 100 m beneath the present land surface by the Archean Biosphere Drilling Project (ABDP-1). The goal of ABDP was to obtain samples below surface

* Corresponding author at: Department of Geoscience, University of Wisconsin-Madison, 1215 W. Dayton Street Madison, WI 53706, United States. Tel.: +1 6087727386.
E-mail addresses: wli@geology.wisc.edu, liweiq@gmail.com (W. Li).

0012-821X/$ – see front matter © 2011 Elsevier B.V. All rights reserved.
doi:10.1016/j.epsl.2011.12.035

weathering zones. The widespread use of drill core to recover fresh samples from Archean terranes is well documented in the literature, and so it was certainly a reasonable expectation that the ABDP-1 core would be free of the effects of recent weathering. In addition, Kato et al. (2009) studied the same drill core and obtained a 2.76 Ga Re–Os age for pyrite hosted in the oxidized Apex Basalt that overlies the MBC. Kato et al. (2009) argued that the co-existence of some pyrite grains with hematite in the drill core indicates oxidation occurred before pyrite formation. They therefore, interpreted the hematite to reflect high-O_2 levels prior to 2.76 Ga, an interpretation that requires that the samples escaped post-Archean weathering. The Australian continent has been exposed since the Triassic (Anand, 2005), which has produced deep weathering in Western Australia (Anand and Paine, 2002). Although samples from ABDP-1 generally lie below the zone of intense Phanerozoic weathering, deep penetration of groundwater in the Phanerozoic remains a possibility.

In this study, we revisited the same ABDP-1 drill core studied by Hoashi et al. (2009) and Kato et al. (2009), who argued that the core preserves Archean oxidation products. We applied U–Th–Pb geochronology to the Apex Basalt samples to determine if oxidation can be confidently constrained to Archean time in the ABDP-1 drill core. Because the Pb–Pb method may produce ambiguous results, we have analyzed U, Th, and Pb concentrations by isotope dilution mass spectrometry, allowing construction of ^{238}U–^{206}Pb, ^{235}U–^{207}Pb, and ^{232}Th–^{208}Pb isochrons to separate mixing relations from geochronologic relations. Our results show that the U–Th–Pb isotope system has been disturbed by U and Pb addition, that U addition correlates with iron oxidation, and that this probably occurred in the last 200 Ma. These results bear on the confidence that drill core escaped recent weathering, and also bear on the interpretation that oxidation of the Apex Basalt occurred in the Archean.

2. Geological background and samples

The Archean Pilbara craton is a granite–greenstone terrane located in northwestern Australia that has been little affected by subsequent metamorphism (Fig. 1A), in which the East Pilbara Terrane is one of the best preserved segments of early Archean crust. The 3.52–3.17 Ga East Pilbara Terrane is composed of granitic intrusions and volcano-sedimentary rocks of the Pilbara Supergroup (Van Kranendonk et al., 2002, 2007b). The Warrawoona Group comprises the lowest stratigraphic part of the Pilbara Supergroup (Fig. 1B), and is the subject of this study. Pillow basalts and well-layered cherts within the Warrawoona Group indicate that at least some sedimentation took place in a deep marine environment (Van Kranendonk et al., 2007b). The Marble Bar Chert (MBC) is the most prominent chert unit in the Warrawoona Group. It is generally 100–200 m thick, and in outcrop stretches north–south over 30 km, west of the town of Marble Bar (Fig. 1A). The MBC is underlain by basalt of the Duffer Formation and overlain by the Apex Basalt (Fig. 1A, B). A bedding-parallel shear zone developed at the contact between the MBC and the less rigid Apex Basalt (Kato et al., 2009), possibly reflecting multiple stages of tectonic deformation between 3.3 Ga and 2.9 Ga (van Haaften and White, 1998; Van Kranendonk et al., 2007b).

The samples analyzed in this study, as well as by Hoashi et al. (2009) and Kato et al. (2009), are from the first diamond drill core of the Archean Biosphere Drilling Project (ABDP-1). The ABDP-1 drilling site is located about 4 km southwest of the town of Marble Bar (Fig. 1A). The 260 m deep drill core of ABDP-1 intersects basalts of the 3.474–3.463 Ga Duffer Formation, the MBC, and the 3.46 Ga Apex Basalt (Fig. 1B, C). In the drill core, the Apex Basalt that is close to the contact with the MBC contains bedding-parallel hematite-rich bands, whereas the basalt of the Duffer Formation near the contact with the MBC contains bedding-parallel goethite-rich bands (Kato et al., 2009; Fig. 1C). These reddish hematite- or goethite-rich basalts are interbedded with less oxidized, green-colored basalts. These relations are well illustrated in surface outcrops (Appendix 1), which indicate that the Apex Basalt was not pervasively oxidized, but preferentially altered along flow margins and deformation zones. The samples analyzed in this study, selected and provided by Prof. Hiroshi Ohmoto and Dr. Yumiko Watanabe from Pennsylvania State University, cover a wide range of oxidation state ($Fe^{(III)}/Fe_{Total}=0.09$–$1.00$; Table 1). Twelve of the thirteen samples analyzed are from the Apex Basalt and include both red hematite-bearing and green non-oxidized samples at core depths of 190–262 m. In addition, one sample of non-oxidized basalt from the Duffer Formation at 42.6 m core depth was analyzed (Fig. 1C).

3. Methods

The drill core was cut and powdered at the Pennsylvania State University. Sample preparation was done to avoid metal contamination, and followed methods used in Hoashi et al. (2009) and Kato et al. (2009). Briefly, core samples ~$5\times1\times0.5$ cm were cut and cleaned in distilled water in an ultrasonic bath, and inspected under a binocular microscope for surface contamination. Core sections were analyzed by an XRF core scanner, and samples for whole-rock chemical and U–Th–Pb isotope analysis were powdered in an agate mill. Analyses of U, Th, and Pb isotope ratios were carried out at the University of Wisconsin-Madison Radiogenic Isotope Laboratory. Approximately 100 mg of each powdered sample was dissolved in a capped Teflon beaker using a mixture of 4 ml of double-distilled 29 M HF and 1 ml of Optima® grade 14 M HNO_3 at 130–150 °C for 2 days and then dried overnight. This process was repeated to ensure complete digestion. The samples were subsequently dissolved in 5 ml double-distilled 5 M HCl and each sample was divided into two aliquots; one aliquot was used for Pb isotope analysis and the other was spiked with a mixed ^{235}U–^{229}Th–^{208}Pb tracer to determine U, Th, and Pb concentrations by isotope-dilution mass spectrometry.

Solutions were chemically purified by anion-exchange chromatography (Appendix 2). Total procedural blanks for Pb chemistry was 50–80 pg, which was less than 0.05% of the amount of Pb in the samples. Total procedural blanks for Th and U were <50 pg, which is less than 1% of the amount of Th and U in the samples.

Lead isotope ratios were determined on a VG Instruments *Sector 54* thermal ionization mass spectrometer using a static multi-collector routine and a ^{208}Pb ion signal of 1.7–2.0×10^{-11} A. Lead was loaded onto single Re filaments and run using the Si-gel H_3PO_4 technique. Lead isotope ratios were corrected for mass fractionation by +0.105%/amu, as constrained by long-term measurement of the $^{207}Pb/^{206}Pb$ ratio of NIST SRM-981 and the $^{208}Pb/^{206}Pb$ ratio of NIST SRM-982. External precision of Pb isotope analysis was ±0.057%/amu (2 relative standard deviation, n = 34), based on repeat measurement of SRM-981 and SRM-982 during the analytical session.

Isotopic ratios of $^{235}U/^{238}U$ and $^{229}Th/^{232}Th$ were simultaneously measured using a Micromass *IsoProbe* MC-ICP-MS. Instrumental mass bias was corrected by a sample-standard bracketing technique, using mixtures of Ames Th mixed with NBL-114 natural U ($^{238}U/^{235}U=137.88$) as bracketing standards. The samples were diluted to match the total ion intensity of the standards. There were no memory effects during analysis, as on-peak zero measurements of U and Th remained unchanged after washout between samples. Tailing effects were negligible, and correction for abundance sensitivity did not shift the results outside analytical error.

4. Results

The whole-rock Pb isotope compositions and U, Th, Pb concentrations determined by isotope dilution are reported in Table 1. Lead concentration varies from less than 1 ppm to 58 ppm, and U concentration varies between 0.08 ppm and 1.04 ppm, but the majority of samples have less than 0.5 ppm U. In contrast, Th concentrations

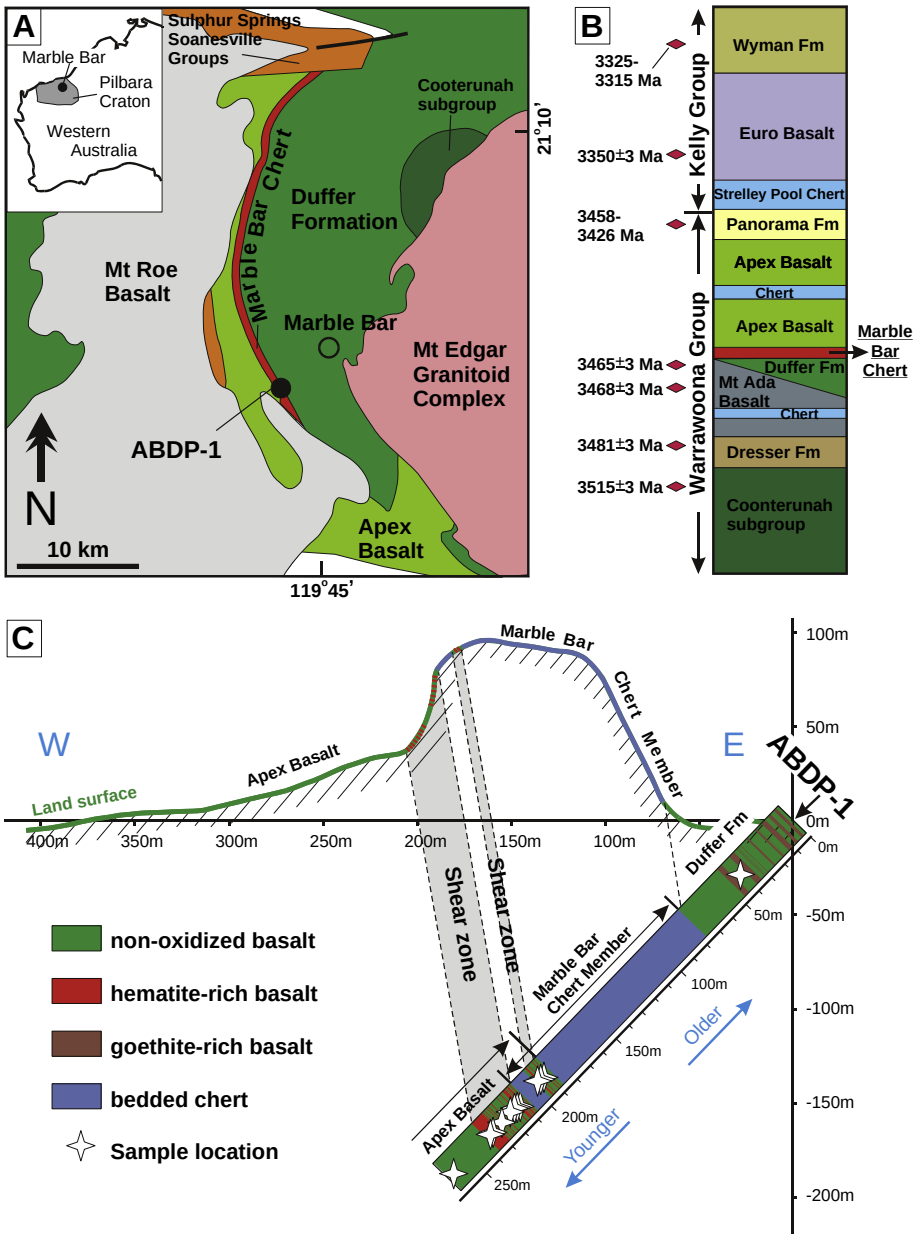

Fig. 1. Geological background of the samples analyzed in this study. Panel A shows the geological map at Marble Bar and the location of the ABDP-1 drill core (modified from Hoashi et al., 2009). Panel B shows the simplified stratigraphic column of the lower part of the Pilbara Supergroup, with ages constrained by zircon U–Pb geochronology (modified from Van Kranendonk et al., 2007b). Panel C shows a schematic cross section of the ABDP-1 drill core (modified from Kato et al., 2009), bedding plane is marked by dash lines along cross section.

Table 1
U–Th–Pb isotopic data of basalt samples from ABDP-1 drill core, Marble Bar, NW Australia.

Sample name [a]	Rock type [a]	$\sum Fe_2O_3$ (wt.%) [a]	$Fe^{(III)}/Fe_{Total}$ [a]	Zr [a] (ppm)	Pb (ppm)	U (ppm)	Th (ppm)	$^{206}Pb/^{204}Pb$	$^{207}Pb/^{204}Pb$	$^{208}Pb/^{204}Pb$	$^{238}U/^{204}Pb$	1SE (%)	$^{235}U/^{204}Pb$	1SE (%)	$^{232}Th/^{204}Pb$	1SE (%)
ABDP-42.60[b]	Tholeiite	13.82	0.25	88	3.14	0.224	0.694	14.661	14.505	34.229	4.002	0.32	0.0290	0.32	12.749	0.34
ABDP-190.26	Tholeiite	7.69	0.90	38	20.97	0.401	0.331	13.730	14.319	33.455	1.043	0.09	0.0076	0.09	0.884	0.13
ABDP-193.28	Tholeiite	1.03	0.64	38	6.73	0.255	0.279	13.273	14.163	32.878	2.030	0.84	0.0147	0.84	2.278	0.84
ABDP-194.17	Tholeiite	1.70	0.84	48	9.82	0.352	0.370	13.662	14.267	33.368	1.950	1.09	0.0141	1.09	2.102	1.12
ABDP-194.44	Tholeiite	9.87	0.98	33	56.01	0.616	0.233	13.303	14.233	33.137	0.592	0.01	0.0043	0.01	0.230	0.08
ABDP-211.40	Tholeiite	9.49	0.75	46	4.07	0.240	0.412	13.425	14.190	33.171	3.182	0.09	0.0231	0.09	5.606	0.13
ABDP-214.13	Tholeiite	28.46	0.58	49	7.40	0.375	0.555	13.011	14.107	32.851	2.700	0.49	0.0196	0.49	4.100	0.50
ABDP-214.18	Tholeiite	34.45	0.93	43	8.50	1.030	0.431	13.203	14.196	33.141	6.517	0.17	0.0473	0.17	2.797	0.19
ABDP-217.80	Tholeiite	19.75	0.09	48	0.77[a]	0.112	0.473	13.954	14.272	33.962						
ABDP-223.25	Tholeiite	7.74	0.12	32	42.55	0.083	0.399	12.413	13.973	32.263	0.102	0.07	0.0007	0.07	0.502	0.06
ABDP-229.45	Tholeiite	19.03	0.66	52	16.46	0.289	0.586	12.560	14.005	32.406	0.920	0.10	0.0067	0.10	1.913	0.11
ABDP-229.60	Tholeiite	4.83	1.00	64	30.08	0.362	0.669	12.493	13.979	32.276	0.629	0.19	0.0046	0.19	1.191	0.19
ABDP-261.45	Tholeiite	11.45	0.27	73	2.30	0.116	0.568	13.742	14.254	34.030	2.785	0.03	0.0202	0.03	13.939	0.26

[a] Provided by Prof. Hiroshi Ohmoto.
[b] Basalt sample from Duffer Formation; other samples are all from the Apex Basalt.

vary little in the samples, ranging from 0.24 ppm to 0.71 ppm (Table 1; Fig. 2B). In general, as $Fe^{(III)}/Fe_{Total}$ ratio increases, U and Pb concentrations increase and become more scattered (Fig. 2A, C), although sample ABDP-1_223.25 m plots off this trend for Pb, where it has a high Pb concentration but low $Fe^{(III)}/Fe_{Total}$ ratio. In contrast, Th content is not correlated with $Fe^{(III)}/Fe_{Total}$ ratios, but is positively correlated with the concentration of immobile elements such as Zr (Fig. 2E) and Ti (not shown). Lead and U contents are not correlated with Zr (Fig. 2D, F), although samples that have low Zr contents tend to have high Pb and U contents. There are no correlations between Pb, Th, or U concentrations with sample depth or major-element compositions such as SiO_2 or Fe_{Total} (not shown).

Relative to average crust (Stacey and Kramers, 1975), the samples analyzed in this study have very low $^{206}Pb/^{204}Pb$, $^{207}Pb/^{204}Pb$ and $^{208}Pb/^{204}Pb$ ratios (Fig. 3A, B). In addition, the Pb isotope ratios are relatively non-radiogenic compared to other Warrawoona Group basalts, as analyzed by Dupré and Arndt (1990) (Fig. 3). The Warrawoona Group basalts have Pb isotope compositions that reflect μ ($^{238}U/^{204}Pb$) value ranges of 4–25, which reflects primary igneous values produced by melting and crystallization processes for fresh basalts (White, 1993). The basalt sample from the Duffer Formation (ABDP-1_42.60 m) has a Pb isotope composition that overlaps with some of the Warrawoona Group basalts, but the Apex Basalt samples have lower $^{206}Pb/^{204}Pb$ ratios that nearly extend to the very non-radiogenic isotope compositions measured in galena from mineral deposits hosted in the Warrawoona Group (Huston et al., 2002; Fig. 3).

On a $^{206}Pb/^{204}Pb$–$^{207}Pb/^{204}Pb$ plot, the Apex Basalt samples scatter about a line that has a slope equivalent to an age of 3067 ± 220 Ma and an MSWD of 8.2 (all best-fit lines calculated using *Isoplot* v2.49 (Ludwig, 1999), where 2–σ errors for Pb isotope ratios are ±0.057%/amu). If the Duffer Formation sample is included in this regression, the fit improves slightly, where the slope of the line is equivalent to an age of 3085 ± 220 Ma (subfigure of Fig. 3B) and an MSWD of 7.6. The age uncertainty can be improved if all the Warrawoona Group basalts are included in the regression; this produces a best fit line that has a slope equivalent to an age of 3209 ± 31 Ma and an MSWD of 16. It is important to note, however, that despite the apparent improvement in the slope precision from addition of all data to the regression, the increase in MSWD indicates a poorer fit relative to analytical uncertainties. In contrast to the apparent ^{207}Pb–^{206}Pb ages, the minimum depositional age of the Warrawoona Group is 3426 Ma based on a U–Pb zircon age from the Panorama Formation, which occurs at the top of the section (van Kranendonk et al., 2007b; Fig. 1B).

5. Discussion

The scatter about the best-fit lines on a $^{206}Pb/^{204}Pb$–$^{207}Pb/^{204}Pb$ diagram (Fig. 3B), as marked by the high MSWD, precludes the samples from representing true ^{207}Pb–^{206}Pb isochrons in the strictest sense, in that the samples could not have evolved from a common source that had the same initial Pb isotope composition, nor remained a closed system with respect to U and Pb. This interpretation is consistent with the fact that the ^{207}Pb–^{206}Pb ages are younger than the depositional age of the basalts based on U–Pb zircon ages. Open-system behavior is well illustrated on plots of $^{206}Pb/^{204}Pb$–$^{238}U/^{204}Pb$ and $^{208}Pb/^{204}Pb$–$^{232}Th/^{204}Pb$ (Fig. 4), which show that the samples do not define linear relations, as would be the case if the samples remained closed since formation. The scatter in the U–Pb and Th–Pb isochron plots can be interpreted to represent U addition and/or addition of Pb of variable isotopic composition (Fig. 4). The mobility of U and Pb in the ABPD-1 samples is well illustrated relative to their Th concentrations, an element that is typically considered immobile, and this is confirmed by the good correlation between Th and Zr contents. The samples analyzed in this study have Th concentrations that are typical for basalts, but their U and Pb concentrations are much higher; for example, typical basalts and komatiites have U/Th and Pb/Th ratios of 0.2–0.3 and 1–6, respectively (Faure, 1986). In contrast, the ABPD-1 samples have U/Th and Pb/Th ratios that range from 0.2 to 2.6 and 2 to 240, respectively (Table 1). Because the U and Pb concentrations increase and become more scattered as $Fe^{(III)}/Fe_{Total}$ ratios increase, we infer that the U and Pb mobilization is associated with the processes that oxidized the Apex Basalt samples. This raises the question: does the linear array for

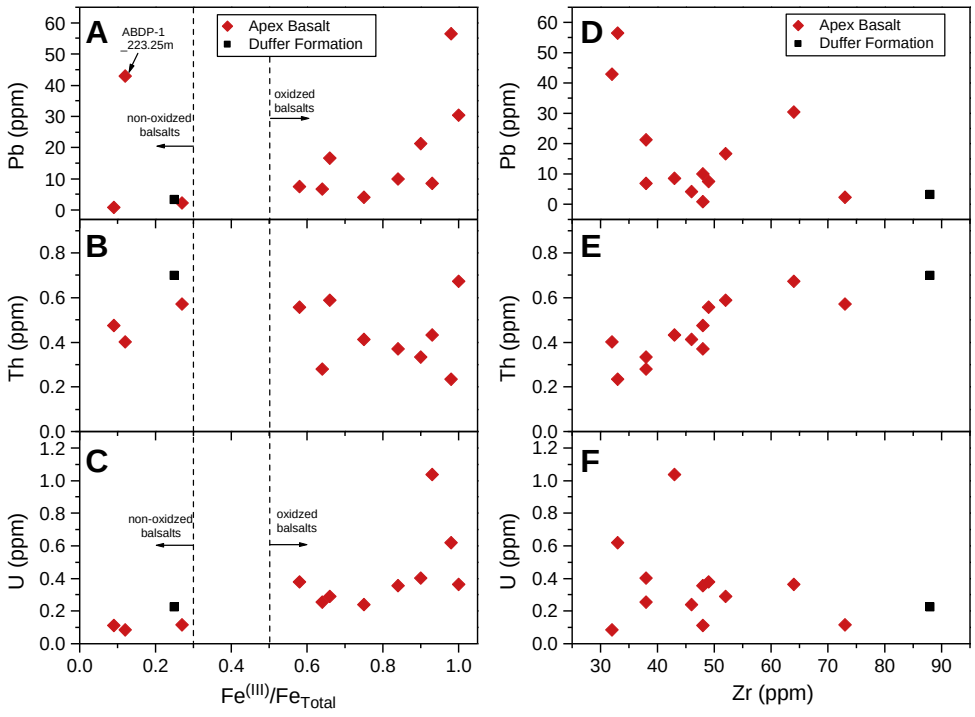

Fig. 2. Concentrations of Pb, Th, and U relative to $Fe^{(III)}/Fe_{Total}$ ratios and Zr content in the basalt samples. The non-oxidized basalts and oxidized basalts are distinguished by the color of rock powders, where non-oxidized basalts are greenish, whereas oxidized basalts are reddish or yellowish.

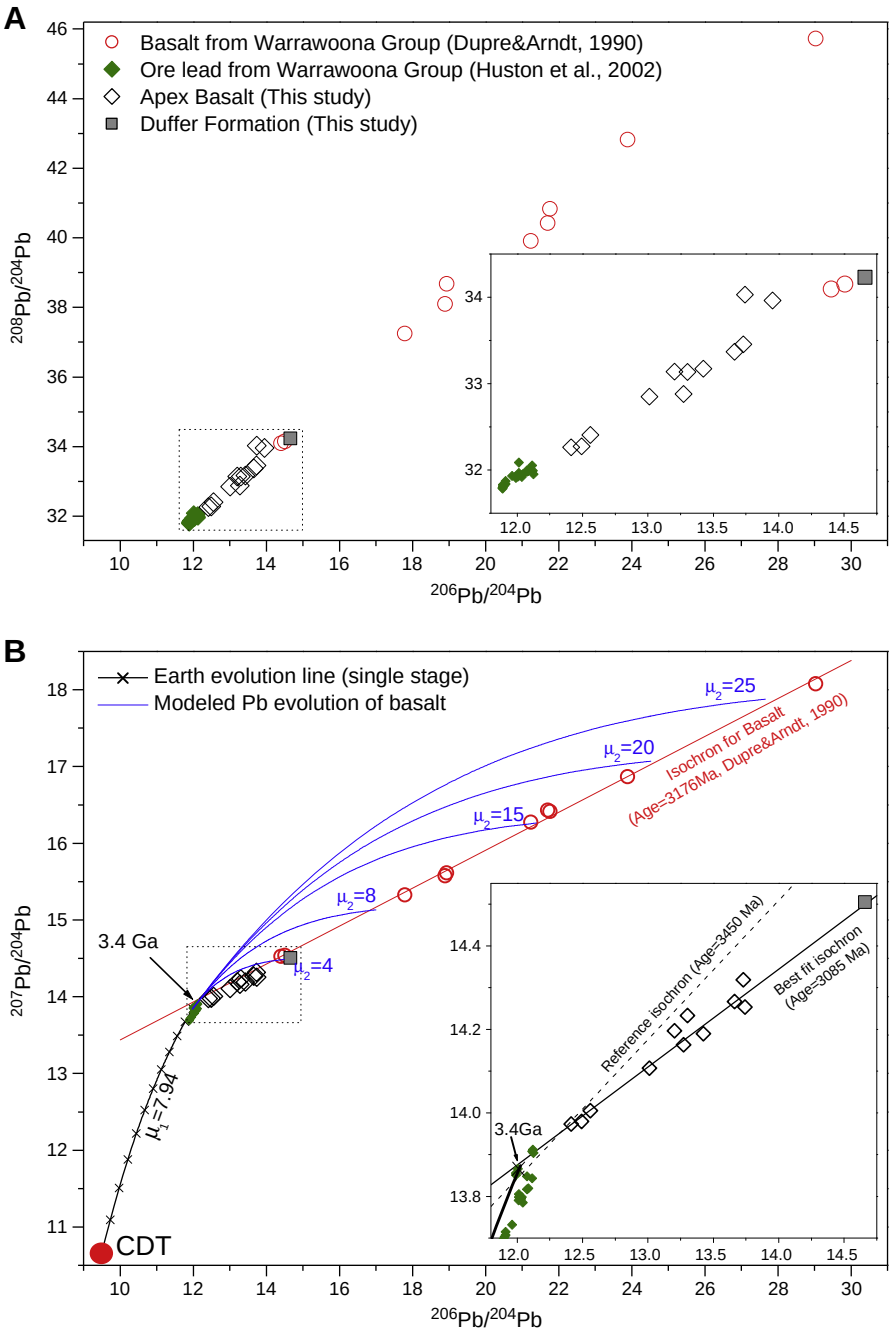

Fig. 3. $^{206}Pb/^{204}Pb$–$^{208}Pb/^{204}Pb$ (A) and $^{206}Pb/^{204}Pb$–$^{207}Pb/^{204}Pb$ (B) variations for basalt samples from ABDP-1 drill core (this study), the Warrawoona Group basalt samples near Marble Bar (Dupré and Arndt, 1990), and ore lead hosted in the Warrawoona Group (complied by Huston et al., 2002). The details of the dashed box are shown in the inset in the lower-left corner of each diagram. For reference, a single-stage Pb growth curve for Earth is shown using an initial Pb isotope composition of Canon Diablo Troilite and a μ_1 value of 7.94. This Pb growth curve fits reasonably well with the ore lead isotope data from the Warrawoona Group, and intercepts the best-fitting isochrons for the basalts from Marble Bar at 3.4 Ga, which is the approximate formation age of these basalts. Secondary Pb growth curves were made using the Pb isotope composition of the primary Pb growth curve at 3.4 Ga as the starting point, and illustrated for μ_2 values between 4 and 25, the same range inferred for the basalts studied by Dupré and Arndt (1990); such a range in μ values matches that of primary (unaltered) basalts (White, 1993). By contrast, the μ_2 values for samples from the ABDP-1 drill core are all below 5.

Apex Basalt samples on a $^{206}Pb/^{204}Pb$–$^{207}Pb/^{204}Pb$ diagram constrain the age of oxidation or is this simply a mixing line that has no age significance? We explore these two possibilities based on two-component mixing calculations and U–Th–Pb isotopic evolution models in the sections below.

5.1. $^{207}Pb/^{204}Pb$–$^{206}Pb/^{204}Pb$ mixing array

We interpret the linear array of $^{206}Pb/^{204}Pb$–$^{207}Pb/^{204}Pb$ data of basalt samples analyzed in this study to be a mixing trend between two Pb end members that have distinct isotopic compositions, rather than an age for oxidation or U–Pb mobilization. Two features of the basalt samples bear on this interpretation. First, compared with basalts of the Warrawoona Group sampled from 40 km south of Marble Bar (Dupré and Arndt, 1990), the Pb in ABDP-1 drill core samples is remarkably less radiogenic (lower in $^{206}Pb/^{204}Pb$, $^{207}Pb/^{204}Pb$; Fig. 3), requiring μ values less than 4, significantly lower than those of fresh basalts (White, 1993). The non-radiogenic nature of this Pb cannot be a result of ancient U depletion, because these samples have high measured U/Th ratios relative to a typical basaltic rock.

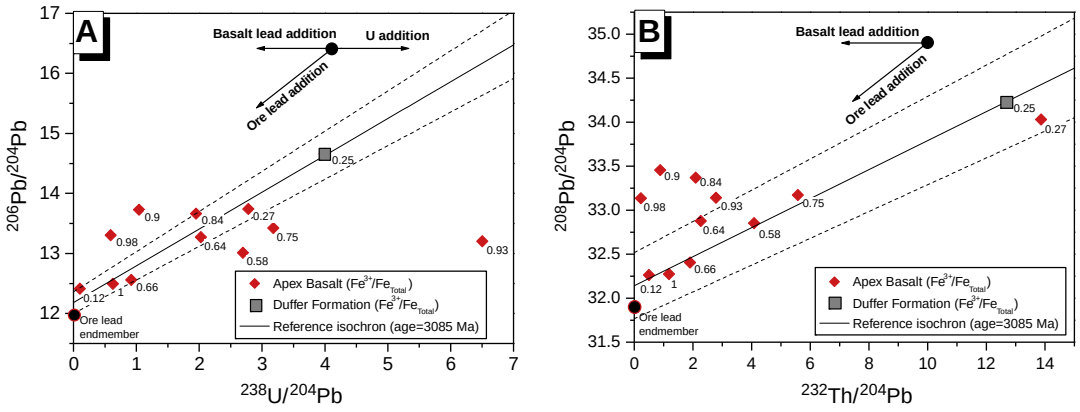

Fig. 4. $^{238}U/^{204}Pb$–$^{206}Pb/^{204}Pb$ (A) and $^{232}Th/^{204}Pb$–$^{207}Pb/^{204}Pb$ (B) variations for basalt samples from the ABDP-1 drill core. The numbers next to the data points denote the degree of oxidation ($Fe^{(III)}/Fe_{Total}$ ratio) for specific samples. The reference isochron corresponds to an age of 3085 Ma, and the dashed lines around the reference isochron represent an age uncertainty of ±220 Ma, as well as uncertainties in initial $^{206}Pb/^{204}Pb$ and $^{208}Pb/^{204}Pb$ ratios of ±0.18 and ±0.38, respectively (see Section 5.2 for details). The isotopic compositions of the "ore lead" endmember are marked in the diagrams. The arrays in the plots show the trajectories a sample would take if influenced by addition of basalt Pb (Warrawoona basalts of Dupré and Arndt, 1990), addition of ore Pb (Warrawoona Group of Huston et al., 2002), or U addition.

Second, Pb contents in the basalts from ABDP-1 drill core are consistently higher than those that are typical for basaltic rocks (typically 0.1–2 ppm; e.g., Hofmann et al., 1986), and, in general, samples that have higher Pb concentration have lower $^{206}Pb/^{204}Pb$ ratios (Table 1; Fig. 5). The anomalously high Pb contents in basalts from the ABDP-1 drill core cannot be solely produced by in situ redistribution of U, Th, and Pb, as would be required for the ^{207}Pb–^{206}Pb array to be an isochron. We therefore conclude that addition of Pb from external reservoirs must have occurred.

The two end members involved in mixing can be conveniently referred to as "basalt lead", defined as the Pb isotope composition of the basalt sample without disturbance, and a non-radiogenic component that is characterized as "ore lead". "Ore lead" is envisioned to be Pb that was separated from the mantle by hydrothermal mineralization events that accompanied magmatic activity during formation of the Warrawoona Group, and was stored in the crust in the form of sulfides, as discussed by Huston et al. (2002). Because ore lead is efficiently separated from U and Th in ore-forming process, the Pb isotope compositions of ore lead are generally taken to be representative of the mantle from which the basalts were derived (Doe, 1970; Doe and Stacey, 1974), which, for the Marble Bar rocks, would be ~3.4 billion years ago. Addition of ore lead at some later time can produce the isotopic compositions of the Apex Basalt samples, including those that have been oxidized, with their characteristic high Pb concentration yet low $^{206}Pb/^{204}Pb$ ratio.

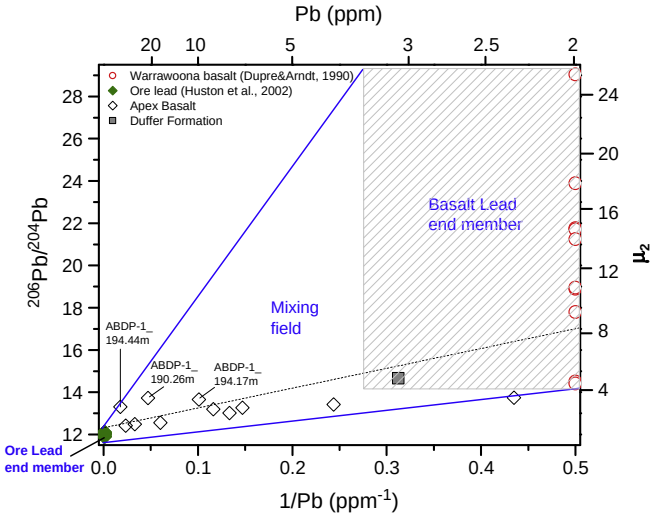

Fig. 5. Mixing relations between $^{206}Pb/^{204}Pb$ and 1/Pb (ppm^{-1}) for basalt samples from the ABDP-1 drill core. The basalt samples analyzed in this study all plot within the mixing field between the "Ore lead" end member and "basalt lead" end member. Names of samples that require high $^{206}Pb/^{204}Pb$ or high Pb concentration for "basalt lead" are denoted next to the data points. The range in $^{206}Pb/^{204}Pb$ ratios correspond to variable μ_2 values in a two-stage Pb growth model as demonstrated in Fig. 3B. For details, see text in Section 5.1.

$^{206}Pb/^{204}Pb$–1/Pb relations for the ABDP-1 basalt samples are shown in Fig. 5, along with fields for ore and basalt lead end members. Two-component mixtures in Fig. 5 are straight lines, and thus components that could have variable Pb isotope compositions or concentrations would define a wedge-shaped mixing field. The field for the ore lead isotope composition is defined by the isotopic composition of galena samples from mineral deposits hosted in the Warrawoona Group (Huston et al., 2002). The Pb concentration was set to be 1000 ppm for the ore lead component, and, at this scale, changes in Pb concentration by a factor of 2–5 do not change the $^{206}Pb/^{204}Pb$–1/Pb relations (Fig. 5). The field for basalt lead is based on the Pb isotope compositions measured in the Warrawoona Group basalts by Dupré and Arndt (1990), and the basalt lead component is arbitrarily portrayed by a field of 2–3.5 ppm Pb. As depicted by the dash line in Fig. 5, the majority of the data can be explained by mixing, between ore lead of $\mu \approx 0$, and basalt lead that had a normal μ value ($\mu_2 \approx 8$) and normal Pb concentrations (<2 ppm). The lower lead concentration limit of the basalt field could be much lower than portrayed, yet still encompass the range of Pb concentration and isotope composition measured for most of the Apex Basalt samples. High Pb concentration or high μ value for the basalt lead field is needed to explain the high Pb concentration of samples at 190.26, 194.17, and 194.44 m core depth.

We conclude that the linear array of Pb isotope data on the $^{207}Pb/^{204}Pb$–$^{206}Pb/^{204}Pb$ diagram is not an isochron, but a mixing line between "ore lead" and "basalt lead". The Pb–Pb array, therefore, has no age meaning. It is important to stress that because the mixing relation lies along the $^{207}Pb/^{204}Pb$–$^{206}Pb/^{204}Pb$ array measured for all Pb sources (ore lead, basalt lead), mixing along the array could have occurred at any time since eruption of the basalts at 3.4 Ga. In other words, "ore lead" addition in the early Archean, or even the Phanerozoic would produce similar Pb–Pb arrays. The timing of "ore lead" addition (mixing), therefore, cannot be constrained from the Pb–Pb isochrons alone.

5.2. Identification of post-depositional processes

The $^{238}U/^{204}Pb$–$^{206}Pb/^{204}Pb$ and $^{232}Th/^{204}Pb$–$^{208}Pb/^{204}Pb$ diagrams (Fig. 4) are further explored to constrain the events of

disturbance of U, Th, and Pb in the samples. The reference isochrons plotted in Fig. 4 reflect an "age" of 3085 Ma, as derived by regression of the ^{207}Pb–^{206}Pb array, and the uncertainty envelope incorporates an age error of ±220 Ma, as well as a variation of ±0.18 and ±0.38 for initial $^{206}Pb/^{204}Pb$ and $^{208}Pb/^{204}Pb$ ratios, respectively. The uncertainty in initial $^{206}Pb/^{204}Pb$ ratio was determined by projection of the isotopic data on the $^{206}Pb/^{204}Pb$–$^{207}Pb/^{204}Pb$ diagram in a direction parallel to the best fit line (isochron of 3085 Ma), to the axis corresponding to an initial $^{207}Pb/^{204}Pb$ ratio of 13.85. This initial Pb composition is based on a single-stage Pb evolution with a μ of 7.98 and an age of 3.4 Ga; this composition overlaps with the Pb isotope composition of Warrawoona galena samples (Huston et al., 2002). The uncertainty in the initial $^{208}Pb/^{204}Pb$ ratio was determined by a similar approach using a $^{208}Pb/^{204}Pb$–$^{206}Pb/^{204}Pb$ diagram and a single-stage growth curve. This approach produces a conservative error envelope with which to judge samples that record element mobilization.

Samples that lie within the uncertainty envelops of the reference isochrons in terms of the ^{207}Pb–^{206}Pb "age" may be explained by mixing between end members that have Pb isotope compositions that lie within the uncertainties noted above (Fig. 4). Because the "ore lead" end member has a Pb isotope composition that is close to the initial Pb isotope composition and $^{238}U/^{204}Pb$ and $^{232}Th/^{204}Pb$ ratios of zero, addition of "ore lead" produces a mixing trend that is subparallel to the reference isochron on $^{238}U/^{204}Pb$–$^{206}Pb/^{204}Pb$ or $^{232}Th/^{204}Pb$–$^{208}Pb/^{204}Pb$ diagrams (Fig. 4); such trends may remain within the isochron error envelope. Samples that lie outside of the isochron error envelopes require a process in addition to Pb–Pb mixing.

The positive correlation between Th and Zr contents in the basalts (Fig. 2) suggests that Th is immobile. This indicates that data points that plot to the left of the isochron envelope in the $^{232}Th/^{204}Pb$–$^{208}Pb/^{204}Pb$ diagram (Fig. 4B) are best explained by addition of Pb that is more radiogenic than the "ore lead", rather than "Th loss". Such radiogenic compositions correspond to "basalt lead" (Fig. 3). Data points that fit this model include samples ABDP-1_190.26 m, ABDP-1_194.17 m, and ABDP-1_194.44 m, and these samples correspond to those that have either high Pb contents or very radiogenic Pb isotope ratios, as shown in Fig. 5. If the average $^{208}Pb/^{204}Pb$ ratio of the "basalt lead" component is close to the lower end of the range measured for the Warrawoona Group basalts by Dupré and Arndt (1990), Pb addition would have been relatively young. To the degree that the present-day $^{208}Pb/^{204}Pb$ ratios of the "basalt lead" component are higher, the age of Pb addition would need to increase to account for radiogenic in-growth.

On the $^{238}U/^{204}Pb$–$^{206}Pb/^{204}Pb$ diagram (Fig. 4A), there are data points that plot to the left and right of the isochron envelop. The three samples that plot to the right of the isochron envelop demonstrate that U addition has occurred, because no significant Pb loss is indicated on the $^{232}Th/^{204}Pb$–$^{208}Pb/^{204}Pb$ diagram. The two data points that lie to the left of the isochron envelop indicate that the effect of possible U addition was exceeded by "basalt lead" addition (decreasing U/Pb ratios) for the two samples. In summary, the timing of Pb mixing is difficult to constrain, but the timing of U mobility is better constrained through comparison of measured and modeled U/Th ratios, which is discussed in the next section.

5.3. Uranium addition and Fe oxidation

The constraints on the time of U addition provide the strongest evidence for recent U mobilization and oxidation of the Apex Basalt. Given the evidence that Th was immobile, the timing of U mobility may be estimated by comparing the measured U/Th ratios with those required to produce the measured $^{208}Pb/^{204}Pb$–$^{206}Pb/^{204}Pb$ variations. It is important to note that, because the measured $^{208}Pb/^{204}Pb$–$^{206}Pb/^{204}Pb$ variations for the samples that reflect mixing between "ore lead" and "basalt lead" essentially lie along the same array (Fig. 3), any mixing trend due to addition of "ore lead" or "basalt lead" will not change the information that may be inferred from the U/Th ratio of the system. We calculate a "model U/Th ratio" for each sample to provide a basis for comparison later with the measured U/Th ration, where the model ratio assumes the sample has remained closed to U and Th since basalt formation at 3.4 Ga. The "model U/Th ratio" therefore is that required to produce the $^{208}Pb/^{204}Pb$ and $^{206}Pb/^{204}Pb$ ratios measured in the samples. This calculation shows that in many cases the measured U/Th ratios are greater than those inferred based on the $^{208}Pb/^{204}Pb$–$^{206}Pb/^{204}Pb$ relations (Fig. 6A).

A plot of model U/Th ratio vs. measured U/Th ratio (Fig. 6B) demonstrates that significant U addition has occurred in 9 of the 13 basalt samples. The model U/Th ratios were calculated in two ways to evaluate the sensitivity of necessary assumptions. One model U/Th ratio is calculated assuming derivation from initial Pb isotope compositions at 3.4 Ga that corresponds to the single-stage growth curve previously noted. A second set of model U/Th ratios was calculated assuming isotopic evolution since 2.7 Ga, corresponding to the Re–Os age determined by Kato et al. (2009) on the same core. The 2.7 Ga model U/Th ratio required a Pb growth curve between 3.4 and 2.7 Ga that had a μ value of 2 to match the non-radiogenic present-day isotopic compositions of the samples; this is an unusually low μ value. Despite the widely different approaches for calculating the model U/Th ratios, the results are quite similar (Fig. 6B), indicating that this is a robust approach.

In Fig. 6B, four of the samples plot along a 1:1 line, regardless of use of a 3.4 or 2.7 Ga model, indicating that these samples have likely remained closed to U and Th since formation. These four samples all have $Fe^{(III)}/Fe_{Total}$ ratios less than 0.3 (Table 1), indicating that they are relatively free of oxidation, confirmed by their green color. Importantly, the 1:1 relation of these four samples holds despite the fact that these samples experienced Pb addition, as discussed above. Moreover, the four samples that have matching model and measured U/Th ratios have $^{208}Pb/^{204}Pb$ and $^{206}Pb/^{204}Pb$ ratios that span the entire range measured in this study (Fig. 6A), which indicates that this result is not an accidental function of some specific isotopic composition.

In contrast, the nine samples that plot at high measured U/Th ratios relative to their model U/Th ratio (Fig. 6B) all have $Fe^{(III)}/Fe_{Total}$ ratios greater than 0.5, indicating that these samples have been oxidized, confirmed by their red color. Fig. 6B, therefore, provides the most powerful evidence in our study that the processes that involved Fe oxidation correspond to U addition. Below we discuss the time constraints on oxidation and U enrichment.

5.3.1. Age of U addition and Fe oxidation

The relatively restricted range in Th/U ratios of mafic igneous rocks, which lies between 3 and 5 (e.g., Faure, 1986; Galer and O'Nions, 1985; Larsen and Gottfried, 1960; Tatsumoto, 1978), allows us to constrain the time of U enrichment that lowered the Th/U ratios of the $Fe^{(III)}$-rich Apex Basalt samples (Fig. 6B). A reference reservoir that has a Th/U ratio greater than 5 is highly unlikely, and this is illustrated on a $^{208}Pb/^{204}Pb$–$^{206}Pb/^{204}Pb$ diagram (Fig. 7) as an "Unlikely zone". Note that in Fig. 7, we cast the discussion in terms of Th/U ratios (rather than U/Th ratios as noted earlier), because this is traditional when discussing Pb–Pb diagrams. A similar "Unlikely zone" can be defined for a Th/U ratio less than 3, although this lower boundary is unimportant because none of the Pb isotope evolution curves in Fig. 7 intersects it. The maximum possible boundaries for Th/U ratios for the reference reservoirs are Th/U = infinity (vertical line in Fig. 7) and Th/U = 0 (horizontal line in Fig. 7). Beyond these boundaries, solutions are not possible because the reservoir would involve decreases in $^{206}Pb/^{204}Pb$ or $^{208}Pb/^{204}Pb$ ratios, and these fields are labeled "Forbidden zones".

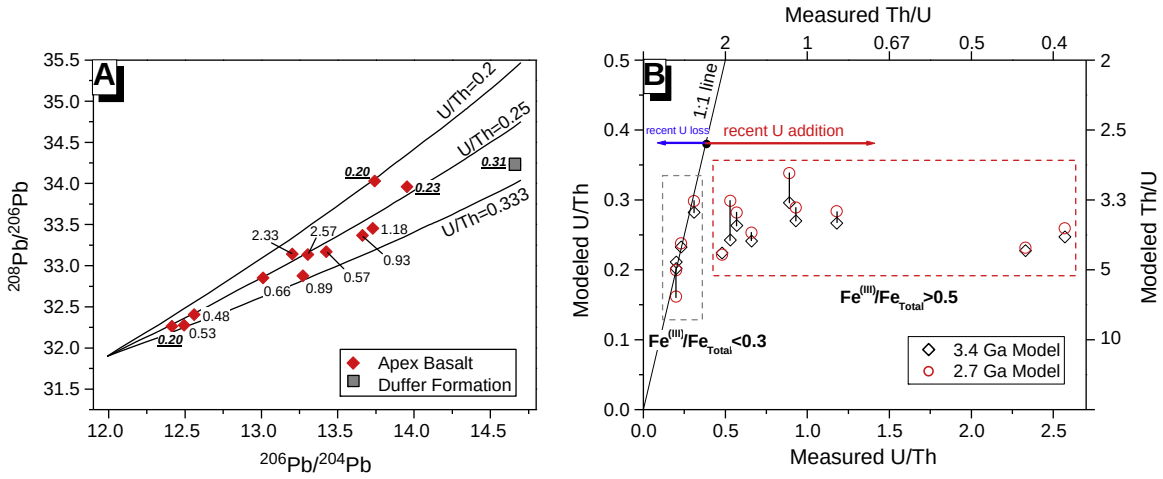

Fig. 6. A: $^{206}Pb/^{204}Pb$–$^{208}Pb/^{204}Pb$ diagram for basalt samples from ABDP-1 drill core. The numbers next to the data points denote the measured U/Th ratio in the basalts. The three lines show the modeled Pb isotope trend if the samples evolved from 3.4 Ga ago with different U/Th ratios but a common starting Pb isotope composition that is the same as the "ore lead". The modeled U/Th ratio that is needed to produce the measured $^{206}Pb/^{204}Pb$ and $^{208}Pb/^{204}Pb$ ratios in each sample can be calculated based on such a plot. B: Plot of modeled U/Th ratio versus measured U/Th ratio for the basalt samples. The "3.4 Ga Model" assumes the system remained closed since 3.4 Ga (as shown in panel A); the "2.7 Ga Model" assumes that the system remained closed since 2.7 Ga. The data require a μ value of 2 between 3.4 and 2.7 Ga, in order to maintain the low, non-radiogenic Pb isotope ratios measured in the samples. Different model results from the same sample are linked with vertical lines. The $Fe^{(III)}/Fe_{Total}$ ratios for the samples are summarized in panel B. These relations provide the most powerful evidence for recent U addition coupled to Fe oxidation. (For interpretation of the references to color in this figure legend, the reader is referred to the web version of this article.)

In calculating the time when the measured Th/U ratios of the samples diverged from various reservoirs, we assume closed-system evolution back in time to intersection with one of the reference Th/U ratios. The Pb isotope evolution trajectory for individual samples on a $^{208}Pb/^{204}Pb$–$^{204}Pb/^{204}Pb$ diagram therefore uses the measured U–Th–Pb isotope compositions (Fig. 7). For the four samples that have low $Fe^{(III)}/Fe_{Total}$ ratios and matching modeled and measured Th/U ratios (samples ABDP_42.60 m, ABDP_217.80 m, ABDP_223.25 m, and ABDP_261.45 m; "1:1 line" in Fig. 6B), the $^{206}Pb/^{204}Pb$–$^{208}Pb/^{204}Pb$ evolution trajectories are parallel to the Th/U trends that are typical of the crust (Appendix 3). In contrast, for the nine samples that have high $Fe^{(III)}/Fe_{Total}$ ratios and were enriched in U (Fig. 6B), the $^{208}Pb/^{204}Pb$–$^{206}Pb/^{204}Pb$ evolution trajectories lie at a lower angle than that of typical crustal Th/U ratios (Fig. 7), and this is exactly what would be expected for recent U enrichment. All the Pb isotope evolution trajectories intersect the boundary of the "Unlikely zone" (Th/U = 5), and the time of intersection varies between 0.2 Ga and 2.6 Ga (Fig. 7). Three of these nine trajectories intersect the boundary of the "Forbidden zone" (Th/U = infinity) at 1.2–2.5 Ga (Fig. 7).

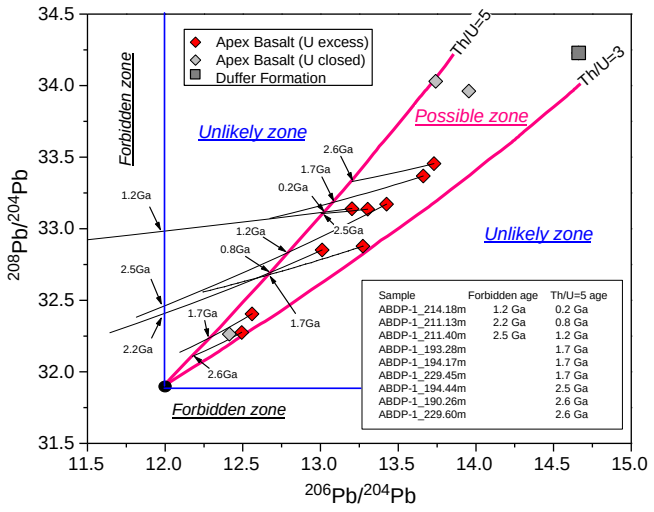

Fig. 7. $^{206}Pb/^{204}Pb$–$^{206}Pb/^{204}Pb$ variations, with illustration of Pb isotope evolution lines, for basalt samples from the ABDP-1 drill core. Red symbols denote oxidized samples that have had U addition and gray symbols indicate samples that are not oxidized. The "Forbidden zone" is defined by $^{206}Pb/^{204}Pb$ < 11.99 or $^{208}Pb/^{206}Pb$ < 31.85, based on the lower limits of the $^{208}Pb/^{204}Pb$ and $^{206}Pb/^{204}Pb$ ratios measured for 3.4 Ga samples discussed in this study. "Possible zone" is divided from the "Unlikely zone" by the Pb isotope trend corresponding to Th/U ratios of 5 and 3, which encompasses virtually all terrestrial basalts. The thin solid lines denote the Pb isotope growth curves back to 2.7 Ga, calculated using the measured U–Th–Pb isotope composition of the samples; curves only shown for oxidized samples (see Appendix 3 for evolution curves for non-oxidized samples). The ages corresponding to interception points between the Pb growth curves and the zone boundaries are marked and tabulated in the diagram. For details, see text in Section 5.3. (For interpretation of the references to color in this figure legend, the reader is referred to the web version of this article.)

The samples that have $Fe^{(III)}/Fe_{Total}$ ratios greater than 0.5 are interpreted to have had variable U enrichment (Fig. 6B), and therefore will contain present-day Pb isotope compositions that reflect variable contributions from Pb that predates the enrichment, and any isotopic response over time after U enrichment. This suggests that the age of U enrichment is best constrained by the highest U/Th samples (samples ABDP_194.44 m and ABDP_214.18 m), for which we calculate a maximum U enrichment age of 2.5 Ga and 0.2 Ga, respectively, assuming a reference reservoir that had a Th/U ratio of 5. It is important to note, however, sample ABDP_194.44 m has the highest Pb concentration, indicating that this sample has a significant ore lead contribution that strongly obscures the isotopic response from U enrichment. We therefore interpret the 0.2 Ga U-enrichment age from sample ABDP_214.18 m to be the maximum age of U enrichment; it is important to note that, this age is a maximum one, because there is no guarantee that we analyzed the samples that experienced the greatest U enrichment and contained the least ore lead component. If samples were analyzed that had higher U/Th ratios, these would produce younger U enrichment ages (in the absence of a large ore lead component) than those measured in this study.

5.4. Implications

5.4.1. Oxidation of the Apex Basalt at ABDP-1 and relations to oxygenation in atmosphere

Uranium was mobilized by oxygen-bearing fluids, given the high solubility of U^{VI} species relative to reduced species (Langmuir, 1978). We infer that U^{VI} was sorbed to the Fe^{3+}-bearing minerals

(hematite and goethite) that are found in the samples, given the high sorption capacity of iron oxides for U^{VI} species in fluids (e.g., Bargar et al., 1999, 2000; Waite et al., 1994; Zeng et al., 2009). Therefore, oxidation of the basalt samples and iron oxide formation were most likely coupled with U enrichment, as demonstrated by the elemental relations in Fig. 6B.

As discussed in the previous section, the most likely maximum age for U enrichment is 0.2 Ga, based on intersection of the Pb isotope growth curves for the high-U/Th, low-Pb sample with a reference reservoir that had a Th/U ratio of 5. A highly conservative, although unlikely age for U enrichment would be <2.5 Ga, based on intersection of the Pb isotope growth curves of three basalt samples (ABDP-1_211.40 m, ABDP-1_214.13 m, and ABDP-1_214.18 m) with the Forbidden zone boundary (Fig. 7). Such old ages, however, are improbable not only because they assume an initial Th/U ratio of infinity, but also because the Apex Basalt at Marble Bar was buried to at least 3 km deep since 2.7 Ga until exposure to air in the Phanerozoic (Thorne, 2001; Van Kranendonk et al., 2007a). In addition, it seems unrealistic to interpret the variable ages in Fig. 7 as reflecting many "events" of U enrichment. Instead, the variable ages are more likely to reflect variable mixtures of end members of U enrichment that is best constrained at <0.2 Ga based on the high-U/Th, low-Pb sample ABDP_214.18 m. Nevertheless, even the highly conservative U-enrichment age estimates based on intersection of the growth curves with the Forbidden zone (Th/U = infinity) are <2.5 Ga, younger than the age estimate for an oxygenated atmosphere of >2.7 Ga, as proposed by Kato et al. (2009).

The Australian continent has been exposed since the Triassic (Anand, 2005), and the weathering processes initiated since then resulted in weathering profiles commonly of 50–100 m deep in Western Australia. Clear weathering profiles up to 150 m have also been reported in the Yilgarn craton (Anand and Paine, 2002). Weathering may extend to deeper levels along structures such as shear zones and faults, which have been shown to greatly increase fluid mobility (Fourcade et al., 1989; Goldblum and Hill, 1992; Huntoon and Lundy, 1979) and enhance weathering (Anand and Paine, 2002; Hickman et al., 1992; Lidmar-Bergström, 1995). Weathering profiles along faults have been reported to reach a depth of 300 m (Olesen et al., 2007). The multi-stage regional deformation history of the Marble Bar area (van Haaften and White, 1998) includes bedding-parallel shear zones near the contact between the Marble Bar Chert and the Apex Basalt, and oxidation of Apex Basalt is commonly localized to shear zones (Kato et al., 2009). In addition, the present bedding of the MBC has an almost vertical orientation (Fig. 1C), which may also facilitate downward infiltration of recent O_2-rich groundwater from the surface. Oxidation of pyrite that occurs in the shear zones (Kato et al., 2009) may provide acidity and porosity that could further enhanced weathering. Such positive feedback by oxidative dissolution of sulfides has been attributed to weathering profiles up to 1 km deep in many Carlin-type deposits (Phillips et al., 1998). It seems possible, therefore, that the Apex Basalt recovered by the ABDP-1 drill core has been partially influenced by recent fluid flow. Weathering that is widespread in the Pilbara craton, which has been exposed to sub-aerial conditions since 0.2–0.5 Ga (Anand, 2005; Dammer et al., 1999; Ostwald, 1993; Weber et al., 2005), seems the most likely cause for iron oxidation and U enrichment in the samples studied. The young oxidation age indicates that these samples do not place constraints on atmospheric oxygenation in the Early Archean.

The coexistence of U-enriched, oxidized basalts with non-oxidized basalts in the ABDP-1 drill core suggests that oxidative fluid flow was heterogeneous. The non-pervasive behavior of oxidation of the Apex Basalt, in outcrop (Appendix 1) or in drill core, may explain the preservation of the 2.76 Ga pyrite grains that coexist with hematite in the ABDP-1 drill core. Juxtaposition of oxides and sulfides is common in weathering profiles of mineral deposits (Phillips et al., 1998, and reference therein), and therefore co-existence of pyrite and hematite may not necessarily imply pyrite formed before hematite, as suggested by Kato et al. (2009). Therefore, the 2.76 Ga Re–Os age of pyrite cannot be used to constrain the age of oxidation.

5.4.2. Pb–Pb versus U–Th–Pb whole-rock geochronology

Whole-rock Pb–Pb geochronology is a widely used technique because it is relatively simple, and may "see through" recent Pb loss and U mobilization (e.g., Faure, 1986). We wish to emphasize that in the case of the Apex Basalt, the Pb–Pb "age" does not reflect the age of oxidation because Pb was added to the rocks. Indeed, it is not uncommon that Pb–Pb geochronology produces ages that are not in accord with the geology of the rocks (e.g., Dupré and Arndt, 1990). This study demonstrates that Pb addition can result in a linear mixing trend on a $^{206}Pb/^{204}Pb$–$^{207}Pb/^{204}Pb$ diagram that may be misinterpreted as an isochron, and a full U–Th–Pb isotope analysis is required to fully understand the source, process, and timing of post-depositional alteration. This study emphasizes that a full U–Th–Pb isotope analysis is an essential approach for understanding old rocks that have had complex histories. We note that this is particularly important with the developing new field of stable U isotope geochemistry. Recent discussions on oceanic anoxia using U contents and isotope compositions in sedimentary rocks (e.g., Brennecka et al., 2011) may be complemented by a full U–Th–Pb isotope analysis to determine whether the U signature is syngenetic or not.

6. Conclusions

Uranium, Th, and Pb isotope analyses of the 3.4 Ga Apex Basalt and Duffer Formation constrain the timing of post-formation oxidation. The whole-rock samples have a wide range in U and Pb concentrations, but comparatively restricted Th contents: <1–58 ppm Pb, 0.08–1.04 ppm U, and 0.24–0.71 ppm Th. The sample suite records various extents of oxidation, as recorded by color and $Fe^{(III)}/Fe_{Total}$ ratios, which vary from 0.1 to ~1.0. Samples that have high $Fe^{(III)}/Fe_{Total}$ ratios contain abundant goethite and hematite as alteration products. The Pb and U concentrations are generally higher than those of typical basaltic rocks, and they correlate positively with the $Fe^{(III)}/Fe_{Total}$ ratios of the samples. In general, these samples are characterized by non-radiogenic Pb isotope compositions, where $^{206}Pb/^{204}Pb$ ratios vary between 12.44 and 14.69. This contrasts with fresh basalts from the Warrawoona Group (Dupré and Arndt, 1990), which are more radiogenic and have μ ($^{238}U/^{204}Pb$) values of ~8 to 25, similar to the range found in modern unaltered basalts that record igneous (melting, crystallization) processes (White, 1993).

Although the Pb isotope compositions of the samples define a linear array in terms of $^{206}Pb/^{204}Pb$–$^{207}Pb/^{204}Pb$ variations, the slope of which is equivalent to a ~3.1 Ga age, this relation is interpreted as a mixing trend between a radiogenic "basalt lead" end member and a non-radiogenic "ore lead" end member. The samples do not form isochrons in terms of $^{238}U/^{204}Pb$–$^{206}Pb/^{204}Pb$, $^{235}U/^{204}Pb$–$^{207}Pb/^{204}Pb$, and $^{232}Th/^{204}Pb$–$^{208}Pb/^{204}Pb$ variations, indicating that the samples have not remained a closed system since formation. Correlated Th–Zr contents indicate that Th was relatively immobile during weathering, as is commonly observed in weathered igneous rocks. The scatter in the U–Pb and Th–Pb isochron diagrams therefore reflect mobilization of U and Pb. The timing of U addition that accompanied oxidation of the samples can be constrained through comparison of the measured U/Th ratios with those required to produce the measured $^{208}Pb/^{204}Pb$–$^{206}Pb/^{204}Pb$ isotope compositions. The modeled U/Th ratios calculated from the Pb isotope compositions are correlated with the extent of oxidation, where samples that have $Fe^{(III)}/Fe_{Total}$ ratios >0.5 underwent the most significant U addition. In contrast, samples that have $Fe^{(III)}/Fe_{Total}$ ratios <0.3 have similar measured and modeled U/Th ratios, indicating negligible U addition. These relations indicate that U addition and basalt oxidation were coupled in the Apex Basalt in the ABDP-1 drill core at the Marble Bar locality.

Based on modeling of Pb isotope evolution trajectories for individual samples using the measured U–Th–Pb isotope data, U addition was most likely to have occurred within the last 200 Ma, which is consistent with the age range for deep weathering of the Pilbara Craton. These results, therefore, do not support the proposal of Kato et al. (2009) that the Apex Basalt was oxidized in the Archean and therefore recorded high atmospheric oxygen at that time. We note that this study places no constraints on the age of jaspers from the Marble Bar Chert that underlies the Apex Basalt. Despite recovery of drill core samples from >200 m depth, our results show that this was not sufficient to avoid oxidation by fluid/rock interaction in the Phanerozoic.

Acknowledgements

We thank Prof. Hiroshi Ohmoto and Dr. Yumiko Watanabe for providing the whole-rock powders of ABDP-1 drill core samples and the major- and trace-element data of these samples. This manuscript benefited significantly from detailed discussions with Prof. Hiroshi Ohmoto; although we note that our interpretation differs from that of Prof. Ohmoto. This study was supported by the NASA Astrobiology Institute.

Appendix A. Supplementary data

Supplementary data to this article can be found online at doi:10.1016/j.epsl.2011.12.035.

References

Anand, R.R., 2005. Weathering history, landscape evolution and implications for exploration. In: Anand, R.R., de Broekert, P. (Eds.), Regolith Landscape Evolution Across Australia. Cooperative Research Centre for Landscape Environments and Mineral Exploration, Perth, pp. 2–40.
Anand, R.R., Paine, M., 2002. Regolith geology of the Yilgarn Craton, Western Australia: implications for exploration. Aust. J. Earth Sci. 49, 3–162.
Bargar, J.R., Reitmeyer, R., Davis, J.A., 1999. Spectroscopic confirmation of uranium(VI) carbonato adsorption complexes on hematite. Environ. Sci. Technol. 33, 2481–2484.
Bargar, J.R., Reitmeyer, R., Lenhart, J.J., Davis, J.A., 2000. Characterization of U(VI)-carbonato ternary complexes on hematite: EXAFS and electrophoretic mobility measurements. Geochim. Cosmochim. Acta 64, 2737–2749.
Berkner, L.V., Marshall, L.C., 1965. On the origin and rise of oxygen concentration in the earth's atmosphere. J. Atmos. Sci. 22, 225–261.
Brennecka, G.A., Herrmann, A.D., Algeo, T.J., Anbar, A.D., 2011. Rapid expansion of oceanic anoxia immediately before the end-Permian mass extinction. Proc. Natl. Acad. Sci. 108, 17631–17634.
Canfield, D.E., 2005. The early history of atmospheric oxygen: homage to Robert M. Garrels. Ann. Rev. Earth Planet. Sci. 33, 1–36.
Cloud, P., 1972. A working model of the primitive Earth. Am. J. Sci. 272, 537–548.
Dammer, D., McDougall, I., Chivas, A.R., 1999. Timing of weathering-induced alteration of manganese deposits in Western Australia; evidence from K/Ar and 40 Ar/39 Ar dating. Econ. Geol. 94, 87–108.
Dimroth, E., Kimberley, M.M., 1976. Precambrian atmospheric oxygen: evidence in the sedimentary distributions of carbon, sulfur, uranium, and iron. Can. J. Earth Sci. 13, 1161–1185.
Doe, B.R., 1970. Lead Isotopes. Springer-Verlag, Berline, Heidelberg, and New York.
Doe, B.R., Stacey, J.S., 1974. The application of lead isotopes to the problems of ore genesis and ore prospect evaluation: a review. Econ. Geol. 69, 757–776.
Dupré, B., Arndt, N.T., 1990. Pb isotopic compositions of Archean komatiites and sulfides. Chem. Geol. 85, 35–56.
Farquhar, J., Bao, H., Thiemens, M., 2000. Atmospheric influence of earth's earliest sulfur cycle. Science 289, 756–758.
Farquhar, J., Peters, M., Johnston, D.T., Strauss, H., Masterson, A., Wiechert, U., Kaufman, A.J., 2007. Isotopic evidence for Mesoarchaean anoxia and changing atmospheric sulphur chemistry. Nature 449, 706–709.
Faure, G., 1986. Principles of Isotope Geology. John Wiley & Sons, New York.
Fourcade, S., Marquer, D., Javoy, M., 1989. $^{18}O/^{16}O$ variations and fluid circulation in a deep shear zone: the case of the Alpine ultramylonites from the Aar massif (Central Alps, Switzerland). Chem. Geol. 77, 119–131.
Galer, S.J.G., O'Nions, R.K., 1985. Residence time of thorium, uranium and lead in the mantle with implications for mantle convection. Nature 316, 778–782.
Garrels, R.M., Perry, E.A., Mackenzie, F.T., 1973. Genesis of Precambrian iron-formations and the development of atmospheric oxygen. Econ. Geol. 68, 1173–1179.
Goldblum, D.R., Hill, M.L., 1992. Enhanced fluid flow resulting from competency contrast within a shear zone: the garnet ore zone at Gore Mountain, NY. J. Geol. 100, 776–782.
Hickman, A.H., Smurthwaite, A.J., Brown, I.M., Davy, R., 1992. Bauxite mineralisation in the Darling Range, Western Australia. Geological Survey of Western Australia Report, 33, pp. 1–82.
Hoashi, M., Bevacqua, D.C., Otake, T., Watanabe, Y., Hickman, A.H., Utsunomiya, S., Ohmoto, H., 2009. Primary haematite formation in an oxygenated sea 3.46 billion years ago. Nat. Geosci. 2, 301–306.
Hofmann, A.W., Jochum, K.P., Seufert, M., White, W.M., 1986. Nb and Pb in oceanic basalts: new constraints on mantle evolution. Earth Planet. Sci. Lett. 79, 33–45.
Holland, H.D., 1984. The Chemical Evolution of the Atmosphere and Oceans. Princeton University Press.
Holland, H.D., 1999. When did the Earth's atmosphere become oxic? A reply. Geochem. News 100, 20–22.
Holland, H.D., 2006. The oxygenation of the atmosphere and oceans. Philos. Trans. R. Soc. Lond. B Biol. Sci. 361, 903–915.
Huntoon, P.W., Lundy, D.A., 1979. Fracture-controlled ground-water circulation and well siting in the vicinity of Laramie, Wyoming. Ground Water 17, 463–469.
Huston, D.L., Sun, S.-S., Blewett, R., Hickman, A.H., Kranendonk, M.V., Phillips, D., Baker, D., Brauhart, C., 2002. The timing of mineralization in the Archean North Pilbara Terrain, Western Australia. Econ. Geol. 97, 733–755.
Kasting, J.F., 1993. Earth's early atmosphere. Science 259, 920–926.
Kato, Y., Suzuki, K., Nakamura, K., Hickman, A.H., Nedachi, M., Kusakabe, M., Bevacqua, D.C., Ohmoto, H., 2009. Hematite formation by oxygenated groundwater more than 2.76 billion years ago. Earth Planet. Sci. Lett. 278, 40–49.
Langmuir, D., 1978. Uranium solution-mineral equilibria at low temperatures with applications to sedimentary ore deposits. Geochim. Cosmochim. Acta 42, 547–569.
Larsen, E.S., Gottfried, D., 1960. Uranium and thorium in selected suites of igneous rocks. Am. J. Sci. 258, 151–169.
Lidmar-Bergström, K., 1995. Relief and saprolites through time on the Baltic Shield. Geomorphology 12, 45–61.
Ludwig, K.R., 1999. Using Isoplot/Ex, Version 2.01: a geochronological toolkit for Microsoft Excel. Berkeley Geochronology Center Special Publication, 1a, pp. 1–47.
Ohmoto, H., 1997. When did the Earth's atmosphere become oxic? Geochem. News 93 (12–13), 26–27.
Ohmoto, H., Watanabe, Y., Ikemi, H., Poulson, S.R., Taylor, B.E., 2006. Sulphur isotope evidence for an oxic Archaean atmosphere. Nature 442, 908–911.
Olesen, O., Dehls, J.F., Ebbings, J., Kihle, O., Lundin, E., 2007. Aeromagnetic mapping of deep-weathered fracture zones in the Oslo region — a new tool for improved planning of tunnels. Nor. J. Geol. 87, 253–267.
Ostwald, J., 1993. Manganese oxide mineralogy, petrography and genesis, Pilbara Manganese Group, Western Australia. Miner. Deposita 28, 198–209.
Phillips, G.N., Thomson, D.F., Kueth, C.A., 1998. Deep weathering of deposits in the Yilgarn and Carlin gold province. In: Taylor, G., Pain, C. (Eds.), Regolith '98, New Approaches to an Old Continent, 3rd Australian Regolith Conference. CRC LEME Proceedings, Kalgoorlie, Western Australia, pp. 1–22.
Rasmussen, B., Buick, R., 1999. Redox state of the Archean atmosphere: evidence from detrital heavy minerals in ca. 3250–2750 Ma sandstones from the Pilbara Craton, Australia. Geology 27, 115–118.
Stacey, J.S., Kramers, J.D., 1975. Approximation of terrestrial lead isotope evolution by a two-stage model. Earth Planet. Sci. Lett. 26, 207–221.
Tatsumoto, M., 1978. Isotopic composition of lead in oceanic basalt and its implication to mantle evolution. Earth Planet. Sci. Lett. 38, 63–87.
Thorne, A.M., 2001. Geology of the Fortescue Group, Pilbara Craton, Western Australia. Geological Survey of Western Australia Bulletin, 114. Perth.
van Haaften, W.M., White, S.H., 1998. Evidence for multiphase deformation in the Archean basal Warrawoona Group in the Marble Bar area, East Pilbara, Western Australia. Precambrian Res. 88, 53–66.
Van Kranendonk, M.J., Hickman, A.H., Smithies, R.H., Nelson, D.R., Pike, G., 2002. Geology and tectonic evolution of the Archean North Pilbara Terrain, Pilbara Craton, Western Australia. Econ. Geol. 97, 695–732.
Van Kranendonk, M.J., Hugh Smithies, R., Hickman, A.H., Champion, D.C., 2007a. Review: secular tectonic evolution of Archean continental crust: interplay between horizontal and vertical processes in the formation of the Pilbara Craton, Australia. Terra Nova 19, 1–38.
Van Kranendonk, M.J., Smithies, R.H., Hickman, A.H., Champion, D.C., 2007b. Chapter 4.1 Paleoarchean development of a continental nucleus: the East Pilbara terrane of the Pilbara Craton, Western Australia. In: van Kranendonk, M.J., Smithies, R.H., Bennett, V.C. (Eds.), Developments in Precambrian Geology. Elsevier, pp. 307–337.
Waite, T.D., Davis, J.A., Payne, T.E., Waychunas, G.A., Xu, N., 1994. Uranium(VI) adsorption to ferrihydrite: application of a surface complexation model. Geochim. Cosmochim. Acta 58, 5465–5478.
Walker, J.C.G., Brimblecombe, P., 1985. Iron and sulfur in the pre-biologic ocean. Precambrian Res. 28, 205–222.
Watanabe, Y., Farquhar, J., Ohmoto, H., 2009. Anomalous fractionations of sulfur isotopes during thermochemical sulfate reduction. Science 324, 370–373.
Weber, U.D., Kohn, B.P., Gleadow, A.J.W., 2005. Muccan Batholith, Eastern Pilbara, Western Australia. In: Anand, R.R., de Broekert, P. (Eds.), Regolith Landscape Evolution Across Australia: a Compilation of Regolith Landscape Case Studies with Regolith Landscape Evolution Models. Cooperative Research Centre for Landscape Environments and Mineral Exploration, Perth, pp. 338–343.
White, W.M., 1993. $^{238}U/^{204}Pb$ in MORB and open system evolution of the depleted mantle. Earth Planet. Sci. Lett. 115, 211–226.
Zeng, H., Singh, A., Basak, S., Ulrich, K.-U., Sahu, M., Biswas, P., Catalano, J.G., Giammar, D.E., 2009. Nanoscale size effects on uranium(VI) adsorption to hematite. Environ. Sci. Technol. 43, 1373–1378.